PHILOSOPHICAL TRANSACTIONS OF THE ROYAL SOCIETY A MATHEMATICAL, PHYSICAL & ENGINEERING SCIENCES

# Numerical Modelling of Turbulent Flow in a Combustion Tunnel

A. F. Ghoniem, A. J. Chorin and A. K. Oppenheim

*Phil. Trans. R. Soc. Lond. A* 1982 **304**, 303-325
doi: 10.1098/rsta.1982.0014

*Phil. Trans. R. Soc. Lond.* A **304**, 303–325 (1982) [ 303 ]
*Printed in Great Britain*

# NUMERICAL MODELLING OF TURBULENT FLOW IN A COMBUSTION TUNNEL

By A. F. Ghoniem, A. J. Chorin and A. K. Oppenheim
*Lawrence Berkeley Laboratory, University of California, Berkeley, California* 94720, *U.S.A.*

(*Communicated by H. Jones, F.R.S. – Received* 25 *February* 1981)

[Plate 1]

## CONTENTS



A numerical technique is presented for the analysis of turbulent flow associated with combustion. The technique uses Chorin's random vortex method (r.v.m.), an algorithm capable of tracing the action of elementary turbulent eddies and their cumulative effects without imposing any restriction upon their motion. In the past, the r.v.m. has been used with success to treat non-reacting turbulent flows, revealing in particular the mechanics of large-scale flow patterns, the so-called coherent structures. Introduced here is a flame propagation algorithm, also developed by Chorin, in conjunction with volume sources modelling the mechanical effects of the exothermic process of combustion. As an illustration of its use, the technique is applied to flow in a combustion tunnel where the flame is stabilized by a back-facing step. Solutions for both non-reacting and reacting flow fields are obtained. Although these solutions are restricted by a set of far-reaching idealizations, they nonetheless mimic quite satisfactorily the essential features of turbulent combustion in a lean propane–air mixture that were observed in the laboratory by means of high speed schlieren photography.

## Introduction

Numerical analysis of turbulent flow has traditionally been based on some form of finite-difference treatment of appropriately averaged Navier–Stokes equations, supplemented by an adequate set of relations to correlate the turbulent flow parameters: the closure model.

For this purpose it is customary to apply first the Reynolds splitting principle to all the dependent variables. Each term in the governing equations is then appropriately averaged. This may involve either time, or ensemble, or Favre-mass averaging, depending on whether one is seeking a steady-state, or time-dependent, or compressible-flow solution. Owing to the nonlinearity of these equations, double correlations of the fluctuating components arise, while the averaging process involves essentially an integration, as a consequence of which a loss of information is incurred. The usual way to remedy this is to introduce a system of relations between the correlations and some mean flow parameters: the closure relations. To obtain a numerical solution, a finite-difference technique is then applied, yielding the description of the flow field in terms of discrete values of its parameters on the nodes of an Eulerian mesh.

The averaging-closure-differencing method (a.c.d.m.) described above has been used in many variations, producing satisfactory results in good agreement with experimental data for a wide assortment of turbulent flow problems. Work in this field has been reviewed recently by Mellor (1979), McDonald (1979), and, with particular reference to modern methods based on the use of the probability density function (p.d.f.), Williams & Libby (1980). These reviews have demonstrated the value of a.c.d.m. as a powerful analytic tool for the study of turbulent combustion.

The a.c.d.m., however, is handicapped by several drawbacks. The following are particularly relevant to the problem at hand.

(i) The averaging process deprives the equations of essential information about the mechanism of turbulence; this necessitates introducing turbulence models on heuristic grounds rather than obtaining information about them from the solution.

(ii) The turbulence model required for the closure relations has to be postulated and the value of its parameters has to be adjusted to match experimental data.

(iii) The finite-difference technique introduces numerical diffusion, which tends to smooth out local perturbations, an effect that is especially harmful at high Reynolds numbers, where regions of substantial shear arise in the flow field; the effect of the a.c.d.m. in this respect is to curtail the Reynolds number, causing the misrepresentation of some of the most essential features of the flow field.

(iv) The effects of exothermic processes of combustion on the flow field are particularly difficult to handle by the a.c.d.m.; as pointed out over five years ago by Williams (1974), these processes cause many fold increases in specific volume and occur at rates that are so high that taking them properly into account in a finite-difference scheme is associated with practically insurmountable difficulties.

All these drawbacks are addressed by the random vortex method (r.v.m.) developed by Chorin (1973). This method was designed to develop a satisfactory approximation to the solution without finite-difference treatment of the equations. Essential features of the flow field governed by the Navier–Stokes equations are mimicked by the action of vortex elements that model the essential ingredients of turbulence, the elementary eddies. Their random walks express the effects of diffusion, while compliance with the tangential boundary condition at the walls is assured by creation of the proper amount of vorticity. A potential flow solution is used at the same time in accordance with the principle of fractional steps to guarantee that the normal boundary condition is satisfied.

The r.v.m. keeps track of the position and strength of all the vortex elements constituting the flow field and is thus essentially grid-less. It is therefore devoid of the smoothing, intrinsic to the

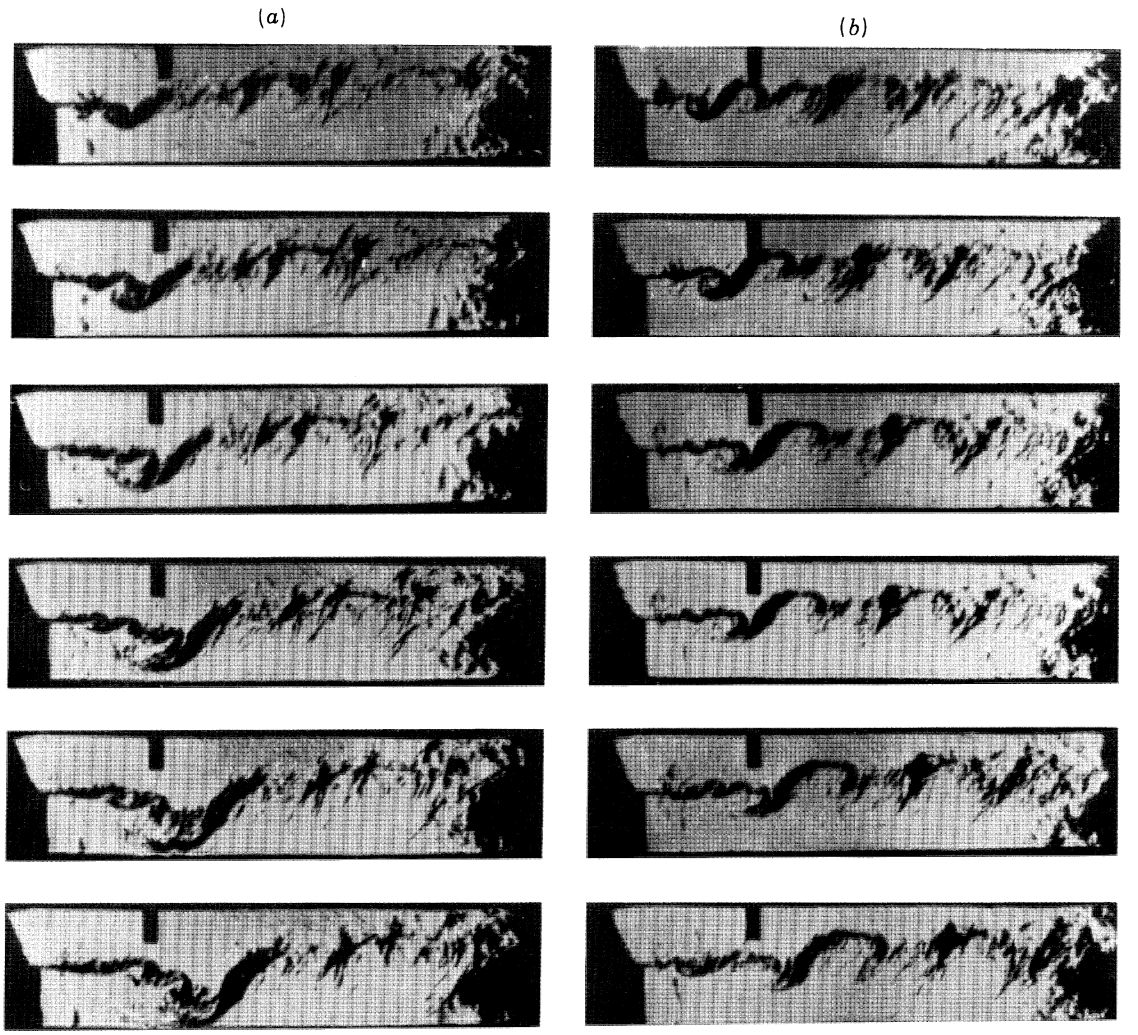


FIGURE 1. Photographic schlieren records of turbulent combustion stabilized behind a step, in a propane–air mixture at an equivalence ratio of 0.57, entering the channel at $u'_\infty = 13.6\ \mathrm{m\ s^{-1}}$ ($R = 22 \times 10^4$) while $T_\infty = 295\ \mathrm{K}$: (*a*) growth of a large eddy under the influence of recirculation (time interval between frames: 1.22 ms); (*b*) 'steady-state' propagation of a large-scale ('coherent') structure (time interval between frames: 1.16 ms).

(*Facing p.* 305)



PHILOSOPHICAL TRANSACTIONS OF THE ROYAL SOCIETY A MATHEMATICAL, PHYSICAL & ENGINEERING SCIENCES

finite-difference technique, and unaffected by the numerical diffusion it introduces. Above all, the r.v.m. does not involve any averaging whatsoever. On the contrary, instead of damping the disturbances, it actually introduces some randomness, or numerical noise, simulating the mechanism of local perturbations in a real flow.

Partial convergence proofs for the r.v.m. have been provided by Chorin *et al.* (1978) and Hald (1979). In particular, the error in the solution was shown to be proportional to the inverse of the square root of the Reynolds number, furnishing further evidence of the eminent suitability of the r.v.m. to the analysis of turbulent flows. Its success in this respect has been amply demonstrated by solutions obtained for flows around solid bodies (Chorin 1973; Cheer 1979), shear layer effects (Ashurst 1979, 1981) and internal flows (McCracken & Peskin 1980). As pointed out by Roshko (1976), it was indeed instrumental in revealing the mechanics of large-scale turbulence patterns, the so-called 'coherent structure', by elucidating such features as the shear layer mechanism and the processes of eddy shedding, growth, intertwining, and pairing.

The most prominent aspects of the r.v.m. are presented here from an entirely pragmatic point of view. The algorithm, augmented to accommodate the effects of flames, is then applied to the analysis of turbulent flow with combustion stabilized in the recirculation zone behind a step.

Salient features of such a flow field are displayed in figure 1 (plate 1), a selection of photographic schlieren records presented by Ganji & Sawyer (1980). The large-scale vortex pattern characteristic of the 'coherent structure' is clearly discernible, while the flame front is recorded by dark streaks, the loci of maximum gradient in the refractive index reflecting the rapid change in density and temperature due to combustion. The records were obtained for a propane–air mixture at an equivalence ratio of 0.57, initial temperature of 295 K flowing at a velocity of 13.6 m $s^{-1}$ (Reynolds number $2.2 \times 10^4$) in the inlet channel, 2.54 cm wide, into a test section 5.08 cm wide and 17.3 cm deep. There are two sequential series made out of extracts from the same high speed film. Series (*a*) shows the process of the coalescence of eddies and their intrusion into the recirculation zone, the time interval between frames being 1.22 ms. Series (*b*) shows the normal formation and development of eddies in the mixing zone, the time interval between frames being 1.16 ms.

The analysis is restricted by a formidable array of simplifying idealizations. The most important among them is the restriction to two-dimensional flow fields, as a consequence of which many interesting features of turbulence cannot be treated. It should be stressed, however, that this is not tantamount to limitations of the r.v.m. itself. In fact it has been recently extended and applied to the study of boundary layer transition in a three-dimensional flow field (Chorin 1980*a*). The principal *raison d'être* for our idealizations is simplicity, for in the first practical application of a new method the simplest example is most appropriate. Simplicity, moreover, provides for economy in computations. The computational techniques developed on this basis should be of benefit to future work on more involved problems.

## *Notation*

| | | | |
|---|---|---|---|
| $A$ | area | $f$ | $V_b/V_c$, fractional volume of burned medium in a cell |
| $c$ | $(T-T_u)/(T_b-T_u)$, reaction progress parameter or reactedness | $F$ | $d\zeta/dZ$, differential transformation function |
| $d_j$ | influence factor of a vortex sheet | | |

$h$ length of a vortex sheet
$h_c$ side length of a cell
$G$ Green function
$H$ width of the channel
$k$ time step
$L$ reference length
i $(-1)^{\frac{1}{2}}$
$J_b$ number of vortex blobs
$J_s$ number of source blobs
$\boldsymbol{n}$ unit vector normal to solid boundaries
$p$ $p'v'/\boldsymbol{u}'_\infty$, non-dimensional pressure
$p'$ pressure
$\boldsymbol{r}$ $(x, y)$, position vector
$r_0$ blob core radius
$R$ $\boldsymbol{u}'_\infty H/2v'\mu$, Reynolds number
$\boldsymbol{s}$ unit vector tangential to solid walls
$S$ normal burning velocity
$t'$ time
$t$ $t'\boldsymbol{u}'_\infty/L$, non-dimensional time
$T$ temperature
$\boldsymbol{u}$ $(u, v)$ non-dimensional velocity vector
$u$ non-dimensional velocity component in the $x$-direction
$\boldsymbol{u}'_\infty$ inlet velocity
$v$ non-dimensional velocity component in the $y$-direction
$v'$ specific volume
$V$ volume
$W$ $u-iv$, complex velocity
$x, y$ non-dimensional Cartesian space coordinates
$Z$ $x+iy$, complex position coordinate in physical plane

$\gamma$ $\int \xi \, dy$, circulation per unit length
$\Gamma$ $\int \xi \, dA$, circulation
$\delta$ Dirac $\delta$-function
$\delta_s$ thickness of the numerical shear layer
$\Delta$ source strength
$\epsilon$ local rate of expansion
$\zeta$ complex position coordinate in the transformed plane
$\eta$ Gaussian random variable
$\mu$ dynamic viscosity
$\nu$ $T_b/T_u$, temperature, or specific volume ratio
$\xi$ $\nabla \times \boldsymbol{u}$, vorticity
$\sigma$ $(2k/R)^{\frac{1}{2}}$, standard deviation
$\phi$ velocity potential
$\psi$ stream function
$\nabla^2$ Laplacian operator

*Subscripts*

b burnt medium
c cell
f flame front
$i$ point in space
$j$ vortex element
p potential flow produced by $\boldsymbol{u}_\infty$
s source velocity
u unburnt medium
$\epsilon$ produced by combustion
$\xi$ produced by turbulence
$\sigma$ due to combustion

*Superscript*

* complex conjugate

## 1. Problem

According to the arguments presented in the Introduction, the problem we treat is formulated on the basis of the following idealizations:

(i) the flow is two-dimensional, i.e. strictly planar;

(ii) the flowing substance consists only of two incompressible media; the unburned mixture and the burned gas;

(iii) the flame is treated as a constant-pressure deflagration acting as an interface between the two media, and propagating locally at a prescribed normal burning velocity;

(iv) the exothermicity of combustion is manifested entirely by an increase in specific volume associated with the transformation of one component medium into the other.


PHILOSOPHICAL TRANSACTIONS OF THE ROYAL SOCIETY A MATHEMATICAL, PHYSICAL & ENGINEERING SCIENCES

Thus the following physical phenomena are, with respect to each idealization, completely neglected:

(i) three-dimensional effects, in particular vortex stretching;

(ii) compressibility effects, in particular acoustic wave interactions;

(iii) chemical kinetic effects and molecular transport processes, governing the structure of the flame and its propagation velocity, as well as such secondary effects as the generation of vorticity due to the interaction between the density jump across the flame front and the pressure gradient in the flow field;

(iv) thermal effects, in particular all the thermodynamic properties of the substance and the heat transfer processes.

It should be noted that the model described is consistent with the well known model of thin-flame, or infinitely fast kinetics, used widely for the analysis of mixed controlled turbulent combustion.

As a consequence of these idealizations, the continuity and the Navier–Stokes equations governing the flow field can be expressed in the following simple form:

$$\nabla\cdot\boldsymbol{u} = \epsilon(\boldsymbol{r}_f), \tag{1.1}$$

$$D\boldsymbol{u}/Dt = R^{-1}\nabla^2\boldsymbol{u} - \nabla p, \tag{1.2}$$

where $\boldsymbol{u} = (u, v)$ is the velocity vector normalized by the inlet velocity $\boldsymbol{u}'_\infty$, $\epsilon$ is the corresponding local rate of expansion, $\boldsymbol{r} = (x, y)$ is the position vector normalized by $L$, the reference length, $t$ is the time normalized by $L/\boldsymbol{u}'_\infty$, $R$ is the Reynolds number, $p$ is the pressure normalized by $\boldsymbol{u}'_\infty/v'$, $v'$ denoting the initial specific volume of the medium, and subscript f refers to the flame front, while

$$D/Dt = \partial/\partial t + \boldsymbol{u}\cdot\nabla$$

is the substantial derivative, $\nabla^2$ is the Laplacian, and $\nabla$ is the usual differential vector operator.

The flow field is specified by the solution of these equations, subject to the boundary conditions

$$\boldsymbol{u} = 0 \quad \text{along all solid boundaries,} \tag{1.3}$$

$$\boldsymbol{u} = (1, 0) \quad \text{at the inlet.} \tag{1.4}$$

The distribution of $\epsilon$ is determined by the location of the flame front, $\boldsymbol{r}_f$, which is governed by the flame propagation equation

$$\partial\boldsymbol{r}_f/\partial t = S_u\boldsymbol{n}_f + \boldsymbol{u}, \tag{1.5}$$

where $S_u$ is the normal burning velocity, and $\boldsymbol{n}_f$ is the unit vector normal to the flame surface.

## 2. Procedure

The procedure is based on the principle of fractional steps (see, for example, Lie & Engel 1880; Samarski 1962), according to which the governing equations are split into a sum of elementary components, and the solution is determined by treating these components in succession.

The essential element used for this purpose is the vorticity..

$$\xi = \nabla\times\boldsymbol{u}, \tag{2.1}$$

which is introduced by expressing equation (1.2) in terms of its curl, the vortex transport equation,

$$D\xi/Dt = R^{-1}\nabla^2\xi, \tag{2.2}$$

since $\nabla \times \nabla p \equiv 0$.

The flow is thus described by equations (1.1), (2.1) and (2.2).

Equations (1.1) and (2.1) are used to determine the velocity field, $\boldsymbol{u}(\boldsymbol{r})$, while, in accordance with the principal feature of the r.v.m., equation (2.2) is used to update the vorticity field, $\xi(x, y)$. Then $\epsilon(x, y)$ is determined by the flame propagation algorithm we developed for the solution of equation (1.5).

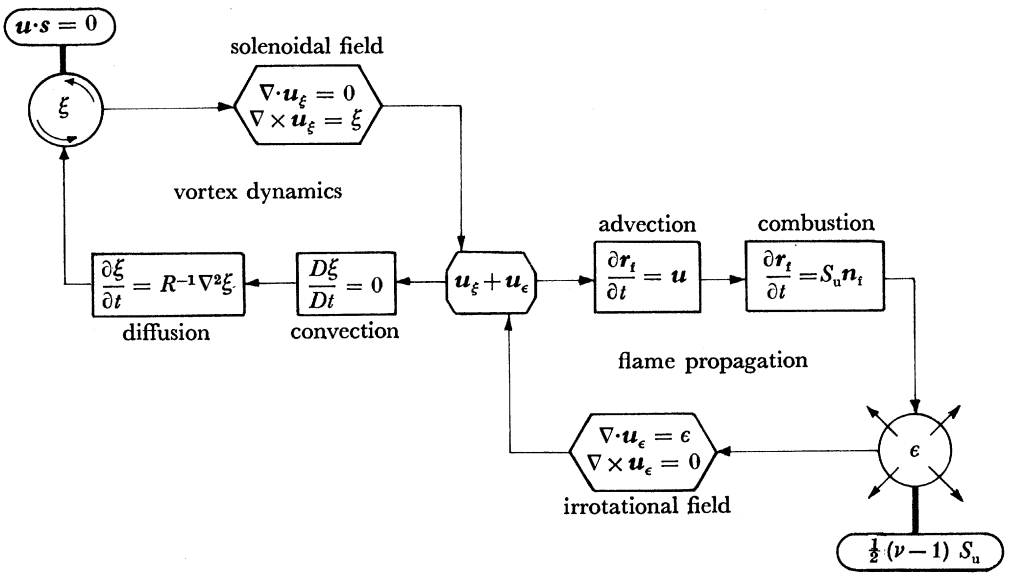


FIGURE 2. Structure of the algorithm.

Thus $\boldsymbol{u}$ is decomposed into a divergence-free vector field $\boldsymbol{u}_\xi$ and a curl-free field $\boldsymbol{u}_\epsilon$, where

$$\boldsymbol{u} = \boldsymbol{u}_\xi + \boldsymbol{u}_\epsilon. \tag{2.3}$$

In doing this, we exploit the Hodge decomposition theorem (see Batchelor 1967; Chorin & Marsden 1979). The governing equations for $\boldsymbol{u}_\xi$ and $\boldsymbol{u}_\epsilon$ are then obtained immediately by the substitution of equation (2.3) in equation (1.1) and (2.1):

$$\nabla\cdot\boldsymbol{u}_\xi = 0, \quad \nabla\times\boldsymbol{u}_\xi = \xi, \tag{2.4, 2.5}$$

and

$$\nabla\cdot\boldsymbol{u}_\epsilon = \epsilon, \quad \nabla\times\boldsymbol{u}_\epsilon = 0. \tag{2.6, 2.7}$$

Both $\boldsymbol{u}_\xi$ and $\boldsymbol{u}_\epsilon$ are required to satisfy independently the zero normal velocity boundary condition, namely

$$\boldsymbol{u}_\xi\cdot\boldsymbol{n} = 0, \quad \boldsymbol{u}_\epsilon\cdot\boldsymbol{n} = 0, \tag{2.8, 2.9}$$

where $\boldsymbol{n}$ is the unit vector normal to the walls.

However, only the total velocity, $\boldsymbol{u}$, is required to satisfy the no-slip condition

$$\boldsymbol{u}\cdot\boldsymbol{s} = 0, \tag{2.10}$$

where $\boldsymbol{s}$ is the unit vector tangential to the walls.

The structure of the algorithm is described schematically in the form of a flow diagram in figure 2. There are two loops, one for handling *vortex dynamics*, and the other for *flame propagation*. These are linked together to yield the total velocity field. Key elements in the first loop are vortices, generated by the no-slip boundary condition at the walls and transported by diffusion and convection, the fractional steps of equation (2.2). Key elements in the second loop are sources of specific volume, generated by the flame propagation process and monitored by combustion, the fractional steps of equation (1.5).

## 3. Vortex dynamics

The mechanism of turbulence is described in essence by vortex dynamics. This process is evaluated here by first determining the velocity field $\boldsymbol{u}$, produced by a given vorticity distribution, $\xi(x, y)$, according to equations (2.4) and (2.5), with the zero normal velocity boundary condition, equation (2.8), and then updating the vorticity field in accordance with the vortex transport equation, equation (2.2), implementing at the same time the non-slip boundary condition, equation (2.10).

As the principal feature of the r.v.m., the flow field is expressed for this purpose in terms of discrete elements, the so-called vortex blobs and vortex sheets. Their properties are presented here in turn.

### (*a*) *Vortex blobs*

To derive the properties of vortex blobs, equation (2.5) is expressed in terms of the stream function, $\psi$,

$$\nabla^2\psi = -\xi, \tag{3.1}$$

where

$$u = \partial\psi/\partial y; \quad v = -\partial\psi/\partial x, \tag{3.2}$$

so that equation (2.4) is satisfied exactly.

The vorticity is then described in terms of

$$\xi_j = \Gamma_j\,\delta(\boldsymbol{r} - \boldsymbol{r}_j), \tag{3.3}$$

where $\delta$ is the Dirac $\delta$-function and

$$\Gamma_j = \lim_{\Delta A_j \to 0} \int_{\Delta A_j} \xi_j \,\mathrm{d}A \tag{3.4}$$

is the circulation of a vortex at $\boldsymbol{r}_j$, while $\xi_j$ is acting on area $\Delta A_j$. The solution of equation (3.1) is given by the Green function

$$G(\boldsymbol{r}, \boldsymbol{r}_j) = (\Gamma_j/2\pi) \ln |\boldsymbol{r} - \boldsymbol{r}_j|, \tag{3.5}$$

representing the field of a potential vortex.

Equation (3.5) can then be used to construct a solution to equation (3.1) for a general distribution of $\xi$ in the form

$$\psi(x, y) = \int_A G(\boldsymbol{r} - \boldsymbol{r}_j)\,\xi(\boldsymbol{r}_j)\,\mathrm{d}A, \tag{3.6}$$

where $A$ is the area of the flow field. The above integral can be evaluated as a sum of all the contributions of $\xi$, after it had been partitioned into discrete elements $\xi_j$. The elementary vorticity, $\xi_j$, is a function of small support that tends to a $\delta$-function as the area where it exists, $\Delta A_j$, approaches zero. This process requires smoothing of the function in equation (3.5) to

eliminate the singularity at its centre (Chorin 1973). Thus the integral in equation (3.6) becomes

$$\psi = \sum_j G_j \Gamma_j, \tag{3.7}$$

in which case

$$\Gamma_j = \int_{\Delta A_j} \xi_j \, \mathrm{d}A,$$

where $\Delta A_j$ is finite, while $G_j$ is the corresponding smooth Green function at $r_j$ (Chorin 1973; Hald 1979).

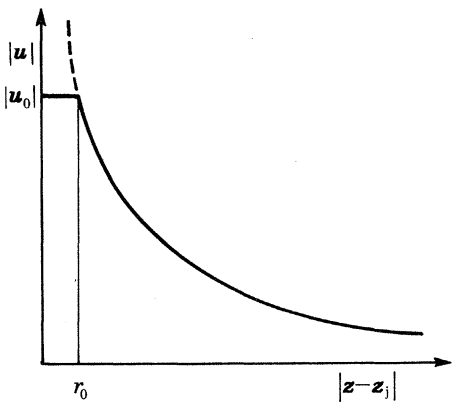


FIGURE 3. Velocity distribution of a blob.

The elementary component of the flow field specified by equation (3.7) is called a vortex blob. The velocity field it produces in a free space, i.e. one without boundaries, is obtained by substituting equation (3.5) into equation (3.2) and smoothing $G$ around the centre. For this purpose the velocity vector is expressed, in terms of complex variables as follows:

$$W_\psi(Z, Z_j) = \frac{-\mathrm{i}\Gamma_j |Z - Z_j|}{2\pi \max(|Z - Z_j|, r_0)} \frac{1}{(Z - Z_j)}, \tag{3.8}$$

where $W = u - \mathrm{i}v$, $\mathrm{i} = (-1)^{\frac{1}{2}}$, $Z = x + \mathrm{i}y$, while $r_0$ is the cut-off radius, i.e. the radius of the core within which $|\boldsymbol{u}|$ is constant, in compliance with the smoothing requirement for the function expressed by equation (3.5). The velocity distribution of a blob is displayed in figure 3.

To satisfy the boundary condition given by equation (2.8), we use conformal mapping to transform the flow field into the upper-half $\zeta$-plane, and add the velocity produced by the image of vortex $\zeta_j$. The corresponding velocity field in the $\zeta$-plane produced by a vortex blob at $\zeta_j$ is thus given by

$$W_\zeta(\zeta, \zeta_j) = W_\psi(\zeta, \zeta_j) - W_\psi(\zeta, \zeta_j^*), \tag{3.9}$$

where $W_\psi(\zeta, \zeta_j)$ is given by equation (3.8), and an asterisk denotes a complex conjugate.

The boundary condition of equation (1.4) is satisfied by the velocity $W_\mathrm{p}(\zeta)$ of the potential flow produced by a unit velocity at the inlet. The total velocity produced by a set of $J_\mathrm{b}$ vortex blobs, including the effect of flow at the inlet, is thus

$$W_\zeta(\zeta) = W_\mathrm{p}(\zeta) + \sum_{j=1}^{J_\mathrm{b}} W_\zeta(\zeta, \zeta_j). \tag{3.10}$$

Then, to deduce the solution in the physical domain, the $Z$-plane, one applies the Schwarz–Christoffel theorem to specify the differential of the transform function,

$$\mathrm{d}\zeta/\mathrm{d}Z = F(\zeta), \tag{3.11}$$

for a given geometry of the flow field. Since

$$W(Z) = W(\zeta)\,F(\zeta), \tag{3.12}$$

the velocity vector, $\boldsymbol{u}_\xi$, in equation (2.3) is thus determined.

The vorticity, $\xi(x, y)$, is updated at every computational time step, $k$, by solving equation (2.2) in fractional steps made up of the contribution of the convection operator

$$D\xi/Dt = 0 \tag{3.13}$$

and that of the diffusion operator

$$\partial\xi/\partial t = R^{-1}\nabla^2\xi. \tag{3.14}$$

According to equation (3.13), vortex blobs move at an appropriate particle velocity specified by equation (2.3).

The solution corresponding to a time step, $k$, of a one-dimensional component of the diffusion equation (3.14), when the initial condition is given by the Dirac delta function, $\delta(0)$, is the Green function

$$G(x, k) = (4\pi k/R)^{-\frac{1}{2}} \exp(-Rx^2/4k). \tag{3.15}$$

This is the probability density function of a Gaussian random variable with zero mean and a standard deviation of $\sigma = (2k/R)^{\frac{1}{2}}$! Thus, if the initial vorticity is split into a set of discrete vortex elements and each is given a displacement from the origin by an amount drawn from a set of Gaussian random numbers of an appropriate variance, it provides an approximation to equation (3.15) by sampling. When a general distribution of vorticity $\xi(x)$ is given, the exact solution of equation (3.14), after a time interval $k$, is

$$\gamma(x) = \int_A G(x-x', k)\,\xi(x')\,\mathrm{d}x' \tag{3.16}$$

where $\gamma$ denotes the circulation per unit length, while $G$ is given by equation (3.15). The probabilistic counterpart of this solution is obtained by displacing each vortex element from its position $x'$ through a distance $\eta_i$. The random walk is then constructed by repeating this procedure at each time step. Two-dimensional random walk is treated in essentially the same way, the vortex elements being moved in two mutually perpendicular directions $x$ and $y$, by two independent Gaussian random variables with zero mean and a standard deviation of $\sigma = (2k/R)^{\frac{1}{2}}$.

The convection and diffusion contributions in the $Z$-plane are combined, according to equation (2.2), by the summation

$$Z_j(t+k) = Z_j(t) + W^*(Z_j)\,k + \eta_j, \tag{3.17}$$

where $W = W_\xi + W_e$ and $\eta_j = \eta_x + \mathrm{i}\eta_y$ or, in the $\zeta$-plane, by using its transform

$$\zeta_j(t+k) = \zeta_j(t) + W^*(\zeta_j)\,F^*(\zeta_j)\,F(\zeta_j)\,k + \eta_j F(\zeta_j). \tag{3.18}$$

Since the velocity is calculated in the $\zeta$-plane by implementing equation (3.10), the use of equation (3.18) is more straightforward and hence more economical than that of equation (3.17).

To satisfy the no-slip boundary condition expressed by equation (1.3), the velocity, $W$, has to be calculated at points along the wall. The points are selected to be a distance $h$ apart along each wall. Wherever the tangential velocity $u$ at wall is not zero, a vortex with a circulation $u_w h$ is created and included in the computations at the next time step, according to equation (3.17) or equation (3.18). However, this procedure of vorticity creation is not accurate since on the average one-half of the newly created blobs are lost through diffusion across the wall. This implies that Kelvin's theorem is not satisfied exactly and the accuracy near the wall is poor. Furthermore, vortex blobs do not provide a good description of the flow near solid walls where velocity gradients are very high, because inside the core of a blob the velocity is considered to be constant. This motivates the introduction of vortex sheets to take up the role of blobs in shear layers at the walls.

### (*b*) *Vortex sheets*

If we take $x$ to be the direction along a wall and $y$ the normal to it, the following two conditions are known to prevail in the shear layer immediately adjacent to the wall:

(i) $$\partial v/\partial x \ll \partial u/\partial y; \tag{3.19}$$

(ii) diffusion in the $x$-direction is negligibly small in comparison to convection in this direction.

A vortex element constructed on the basis of these conditions is referred to as the vortex sheet.

As a consequence of equation (3.19), equation (2.5) is reduced to

$$\xi = -\partial u/\partial y. \tag{3.20}$$

The foregoing, in conjunction with equation (2.4), determines $\boldsymbol{u}_\xi(\boldsymbol{r})$ as follows. Integrating equation (3.20) from $y = \delta_s$, the outer edge of the numerical shear layer at the wall, to $y_i$, one obtains,

$$u_\delta(x_i) - u(x_i, y_i) = -\int_{y_i}^{\delta_s} \xi \, \mathrm{d}y, \tag{3.21}$$

where $u_\delta = u$ at $y = \delta_s$.

The integral in (3.21) can be transformed into a summation by partitioning the value of $\xi$ along $y$ and defining the circulation per unit length of a vortex sheet as

$$\gamma_j = \lim_{\Delta y \to 0} \int_{y_i}^{y_i = \Delta y} \xi \, \mathrm{d}y. \tag{3.22}$$

If a sheet has a length $h$, then its circulation, $\Gamma_j$, is

$$\Gamma_j = h\gamma_j, \tag{3.23}$$

and from equations (3.21) and (3.22) the velocity jump across it, $\Delta u_j$, per unit sheet length is

$$\Delta u_j = \gamma_j. \tag{3.24}$$

Unlike the 'elliptic' flow modelled by vortex blobs, where the effect of each blob extends throughout the field, the zone of influence of a vortex sheet is, as a consequence of equation (3.21), restricted to the 'shadow' below it. This zone is indicated by the regions with vertical hatching in figure 4. Thus, the flow velocity at a point $(x_i, y_i)$, where $y_i < y_j$, is determined by the relation

$$u(x_i, y_i) = u_\delta(x_i) - \sum_j \gamma_j d_j, \tag{3.25}$$

a summation counterpart of equation (3.21) according to equations (3.22) and (3.24), while

$$d_j = 1 - |x_i - x_j|/h$$

is the influence factor of sheet $j$ on point $i$, expressing the fraction of the length of the sheet extending over the zone of dependence over point $i$, indicated by horizontal hatching in figure 4.

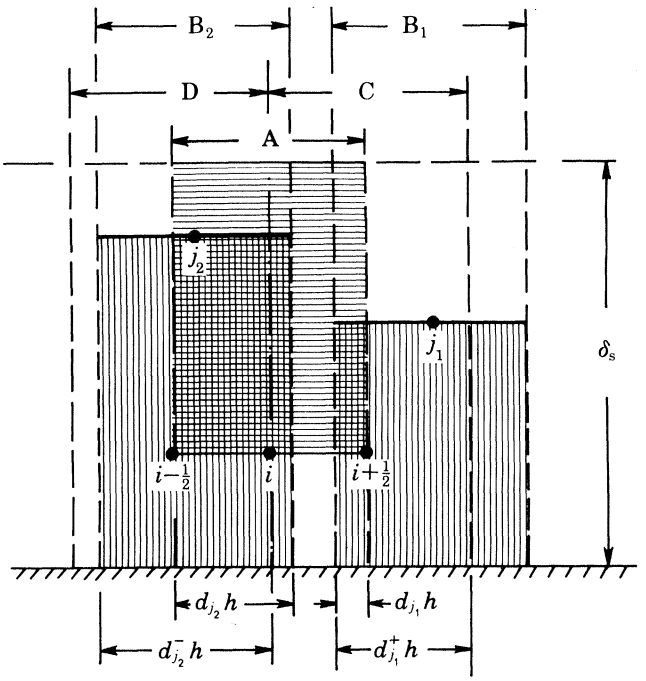


FIGURE 4. Geometry of interdependence in the numerical shear layer: A, zone of dependence over point $i$; B, zone of influence under sheet $j$; C, zone of dependence around point $i+\frac{1}{2}$; D, zone of dependence around point $i-\frac{1}{2}$.

The value of $v$ is determined by the integration of the expression

$$v = -\frac{\partial}{\partial x}\int_0^{y_i} u\,dy, \tag{3.26}$$

obtained from equation (2.4) by using $u(x_i, y_j)$ as evaluated from equation (3.24).

For this purpose we introduce

$$I = \int_0^{y_i} u\,dy = u(x_i)\,y_i - \int_0^{y_i} y\,du = u(x_i)\,y_i - \sum_j \gamma_j d_j y_j, \tag{3.27}$$

where, by taking advantage of equation (3.24), $\Delta u$ has been replaced by $\gamma_j d_j$. In finite-difference form, equation (3.26) then becomes

$$v(x_i, y_i) = -(I^+ - I^-)/h, \tag{3.28}$$

where, according to equation (3.27), by using equation (3.25) for $u(X_i)$,

$$I^{\pm} = u_\delta(x_i \pm \tfrac{1}{2}h)\,y_i - \sum_j y_j^0 \gamma_j d_j^{\pm}, \tag{3.29}$$

while, as indicated in figure 4,

$$d_j^{\pm} = 1 - (x_i \pm \tfrac{1}{2}h - x_j)/h$$

and

$$y^0 = \min(y_i, y_j).$$

The motion of the sheets is governed by an equation identical to (3.17), but with $\boldsymbol{u}$ evaluated from equations (3.25) and (3.29) while $\eta_i = 0 + i\eta_y$, in accordance with condition (ii) stated at the beginning of this section. To make sure that the motion of a vortex sheet is matched with the vortex blob into which it transforms, a correction term of $-\frac{1}{2}\gamma_j$ has to be added to the expression for $u(x_i, y_i)$ given by equation (3.25) to account for the effect of the image of the blob. The paper introducing the vortex sheet method (Chorin 1978) contains information on techniques to reduce the statistical error and speed up the convergence of the algorithm.

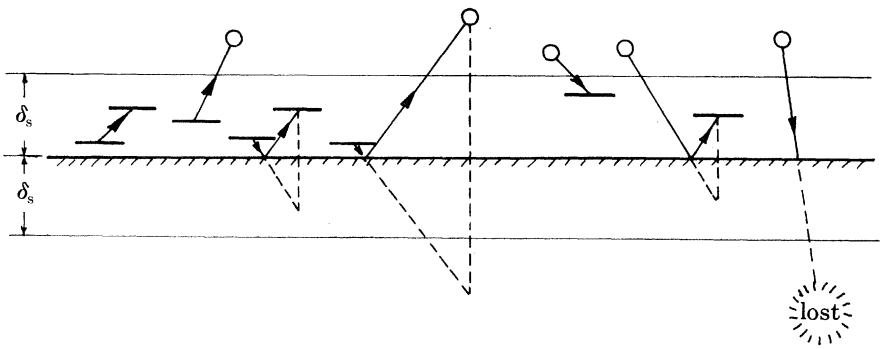


FIGURE 5. Transformations of vortex elements in and around a numerical shear layer at the wall.

### (c) *Algorithm*

The foregoing concepts are implemented as follows.

First the value of $h$, the sheet length specifying the spatial resolution, is chosen. The value of the time step, $k$, is then fixed in accordance with the Courant stability condition, $k \leqslant h/\max|\boldsymbol{u}|$ (Chorin 1980*a*). For a given Reynolds number, this specifies the standard deviation $\sigma$. The thickness of the numerical shear layer $\delta_s$ is then taken as a multiple of $\sigma$ whereby, as shown in figure 5, the loss of vortex blobs due to their random walk is minimized. Finally, the number of sheets initially in the stack is chosen, limiting the maximum allowable value for $\gamma$.

At time zero only the incoming flow $u_p(\zeta)$ exists. The resulting velocity along the wall is fixed by the potential flow solution of equation (3.1). The displacement of the sheets in the numerical shear layer is then calculated, by using equation (3.17) with velocity specified by equations (3.25) and (3.28). The various possibilities that may occur owing to vortex sheet displacement are illustrated in figure 5. When a sheet gets out of the boundary layer, it becomes a blob with a total circulation adjusted according to equation (3.23).

The core radius, $r_0$, is then fixed in such a way that the no-slip boundary condition is satisfied. To do so with a minimum error, one sets $r_0 > \delta_s$. The velocity at the wall produced by the blob and its image is then, in accordance with equation (3.9),

$$u_0 = \Gamma_j/\pi r_0,$$

whence, by virtue of equations (3.23) and (3.24) with $\Delta u_j = u_0$,

$$r_0 = h/\pi, \tag{3.30}$$

providing an explicit relation between the length of the vortex sheet and the core radius of a vortex blob.

If a sheet gets out on the other side of the wall, it becomes restored by its mirror image either in the shear layer as a sheet or in the flow field as a blob, as depicted in figure 5.

Corresponding displacements of vortex blobs are calculated by the use of equation (3.18) with their velocities evaluated from equation (3.10). Again figure 5 displays the various ways in which a blob can be transformed into a sheet. The last possibility of losing a vortex blob is minimized by the right choice of $\delta_s$, as already pointed out.

Once the position and strength of both the sheets and blobs are established, the flow field at a given time step is fully determined. It should be noted that vortex blobs appear only as a consequence of the displacement of vortex sheets outside the boundary layer, modelling the mechanism of the generation of turbulence under actual flow conditions.

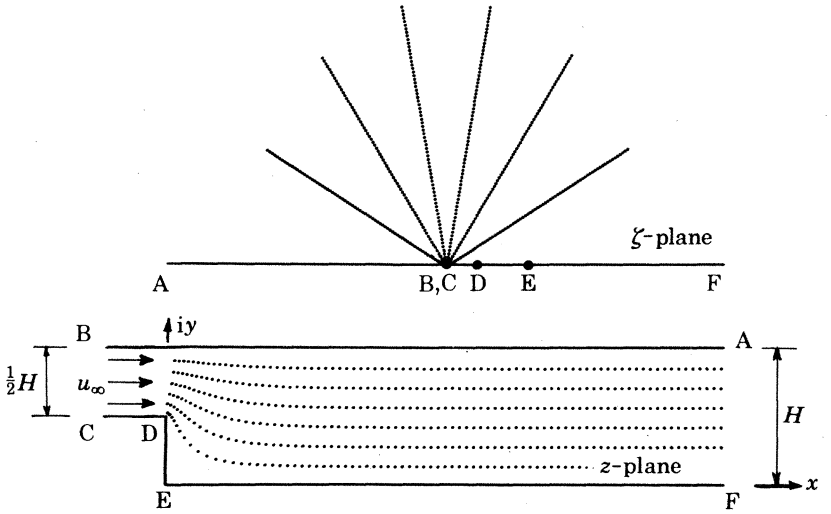


FIGURE 6. Streamlines pattern of initial flow in transformed plane, and physical plane of a channel with a step expansion.

### (*d*) *Results*

The $Z$-plane and $\zeta$-plane for flow over a rearward-facing step are present in figure 6. The functions $W_p$ and $F$ are

$$W_p(\zeta) = H/\pi\zeta \tag{3.31}$$

and

$$F(\zeta) = \frac{\pi\zeta}{H}\left(\frac{\zeta-4}{\zeta-1}\right)^{\frac{1}{2}}, \tag{3.32}$$

where, as shown in figure 6, $H$ is the height of the channel.

The results of computations for turbulent flow behind a step of the same geometrical proportions as figure 1, corresponding to a Reynolds number of $10^4$ at inlet, or for a channel 2.54 cm wide in the experimental apparatus, $u'_\infty = 6$ m s$^{-1}$, are shown in figure 7. Included are two sequential series of computer outputs. Series (*a*) shows the development of the flow field by presenting vortex velocity vector fields tracing the motion of all the vortex blobs included in the solution at successive time intervals, each equal to 50 computational steps of $0.1(H/2u'_\infty)$ s. Series (*b*) shows the growth of a large-scale eddy traced at time intervals equal to five computational steps.

A velocity vector is represented in figure 7 by a line segment providing information on its magnitude and direction. However, instead of being furnished with the conventional arrowhead, it is attached at its origin to a small circle denoting the location of the vortex blob to which it pertains.

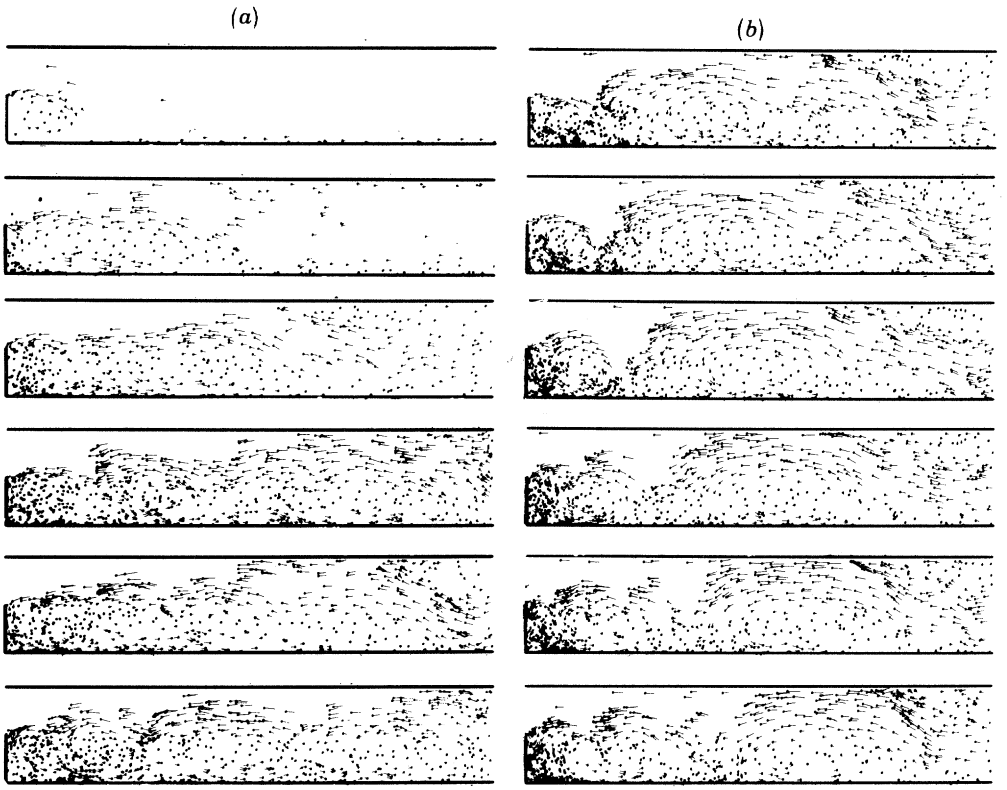


FIGURE 7. Sequential series of computer plots displaying vortex velocity fields in turbulent flow behind a step at inlet Reynolds number $R = 10^4$: (*a*) development of the flow field; (*b*) growth of a large-scale eddy.

## 4. FLAME PROPAGATION

According to idealization (iii), the flame front is treated as an interface across which reactants are transformed into products at a rate controlled by the normal burning velocity. The method used for tracing the motion of such an interface was developed by Chorin (1980*b*) and implemented with the help of the algorithm of Noh & Woodard (1976).

The flow field is divided for this purpose into square cells by a grid of mesh size $h_c$. The fraction of volume, $V$, occupied in a given cell by the burned medium is expressed in terms of a number

$$f \equiv V_b/V_c, \tag{4.1}$$

where subscripts $b$ and $c$ refer, respectively, to the burnt medium and the cell. In terms of specific volumes, $v_i'$ ($i$ = b, c, u, and the last refers to the unburnt medium),

$$f = (1-v_u'/v_c')/(1-v_u'/v_b'). \tag{4.2}$$

Since, because of idealization (iii), the flame is treated as a constant-pressure deflagration, $f$ can be expressed in terms of the usual reaction progress parameter

$$c \equiv \frac{T_c-T_u}{T_b-T_u} = \frac{1}{\nu-1}\left(\frac{T_c}{T_u}-1\right), \tag{4.3}$$

where

$$\nu \equiv T_b/T_u = v_b'/v_u', \tag{4.4}$$

while $T$ can be considered to represent either absolute temperature (if the change in molecular mass is negligible) or temperature divided by the molecular mass.

Thus, with the use of the perfect gas equation of state, equations (4.2), (4.3) and (4.4) yield

$$c = f/\{\nu + (\nu - 1) f\}, \tag{4.5}$$

specifying, in effect, the temperature distribution, for, as a consequence of idealization (ii), $\nu$ is a constant for a given combustible medium.

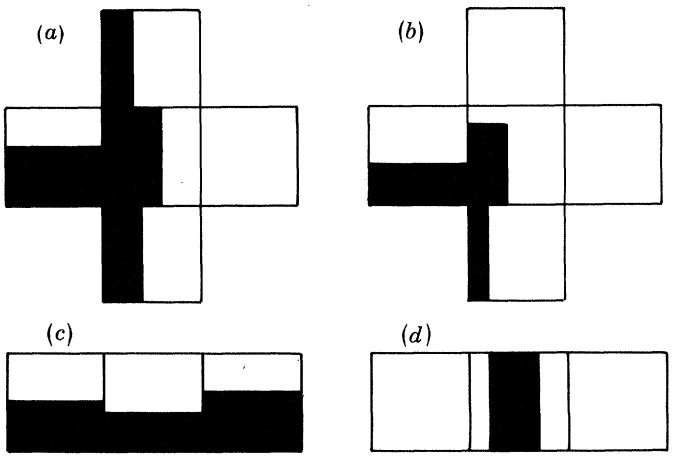


FIGURE 8. Elementary components of an interface recognized by the algorithm.

Thus, $f = 0$, 1 means that there is, respectively, either unburnt or burnt medium in the cell, while fractional values of $f$ indicate cells containing the interface. The particular geometry of the interface is deduced, depending on the $f$-numbers of neighbouring cells. In this connection, as illustrated in figure 8, proper provisions are included in the algorithm for four possibilities:

(*a*) vertical interface;
(*b*) horizontal interface;
(*c*) rectangular corner;
(*d*) neck.

As a consequence, the interface is made up of horizontal and vertical line segments, yielding higher spatial resolution than $h_c$, the mesh size of the grid.

The motion of the interface, or flame propagation, is described by equation (1.5). By virtue of the principle of fractional steps, its effects are split into two components:

(*a*) advection, prescribed by

$$\partial \boldsymbol{r}_f/\partial t = \boldsymbol{u}; \tag{4.6}$$

(*b*) combustion, prescribed by

$$\partial \boldsymbol{r}_f/\partial t = S_u \boldsymbol{n}_f, \tag{4.7}$$

providing a proper set-up for the inclusion of the effects of

(*c*) exothermicity.

Algorithms for each of these processes are presented here in sequence.

### (*a*) *Advection*

The advection step is the passive displacement due to the velocity field. It is evaluated by calculating first the velocity components at mid-points on the sides of the cell, as shown in

figure 9. The interface is then transported in two fractional steps, one horizontal and one vertical, changing the $f$-number of the cell by an amount proportional to corresponding displacements in the time step, $k_c$. The algorithm is stable whenever the Courant condition, $k_c \leqslant h_c/\max|\boldsymbol{u}|$, is satisfied (see Noh & Woodward 1976).

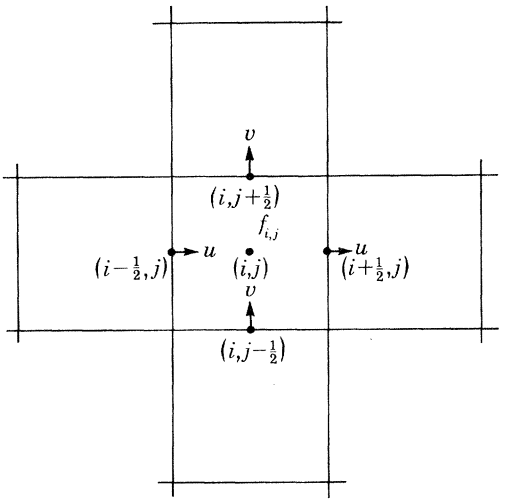


FIGURE 9. Velocity components used in the advection algorithm to determine the motion of the interface in cell $(i,j)$.

### (*b*) *Combustion*

The combustion step is the advancement of the front due to consumption of the unburned medium. The front moves in the direction of its normal with a relative velocity taken here as a constant, equal to the appropriate laminar burning velocity of the mixture, $S_u$. The corresponding motion of the interface is evaluated by the implementation of the Huygens principle, with the use of the advection algorithm. At the $n$th computational step one calculates for this purpose the displacements due to $S_u$ in eight directions – the four sides and four corners of each cell – so that all of the cell's neighbours are affected. For a given cell at $(i,j)$ this results in eight new $f$-numbers. The value assigned to it is then

$$f_{ij}^{n+1} = \max_{0\leqslant l\leqslant 8} f_{ij}^{(l)}, \tag{4.8}$$

where $l = 1, \ldots, 8$, while $f_{ij}^{(0)} = f_{ij}^{n}$. It should be noted that the algorithm provides, in effect, information on the displacement of the interface due to its motion at a given velocity normal to its frontal surface, without having to determine its actual direction (see Chorin 1980*b*).

### (*c*) *Exothermicity*

Mechanical effects of the exothermic process are manifested by volumetric expansion behind the flame front. The velocity field induced thereby is governed by equations (2.6), (2.7) and (2.9).

As for vortex blobs, equations (2.6) and (2.7) are solved by superposition. A velocity potential, $\phi$, is introduced for this purpose, so that

$$u = \partial\phi/\partial x, \quad v = \partial\phi/\partial y, \tag{4.9}$$

satisfying exactly equation (2.7). The governing equation for $\phi$,

$$\nabla^2\phi = \epsilon, \tag{4.10}$$

is then obtained immediately by substitution of equation (4.8) into equation (2.6).

The solution of this equation is given by

$$\phi(r) = \int_A G(r, r')\,\epsilon(r')\,\mathrm{d}A, \tag{4.11}$$

where $G(r, r') = (1/2\pi)\ln|r-r'|$

is the Green function.

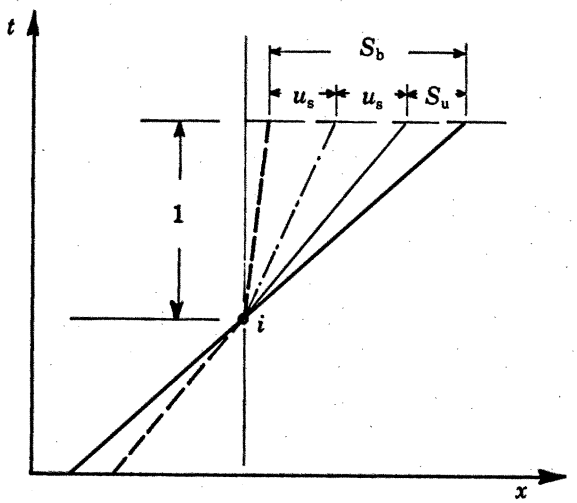


FIGURE 10. Kinematics of the flame front: ——, tangent to the flame front at point $i$; – – –, tangents to particle paths at point $i$.

By following the procedure used for integrating equation (3.6), the solution of equation (4.11) is approximated by the summation

$$\phi = \sum_j G(r, r_j)\,\Delta_j, \tag{4.12}$$

where $\Delta_j$ is the source strength, $\Delta_j = \int_{A_j} \epsilon_j \mathrm{d}A,$ (4.13)

i.e. the rate of volumetric expansion induced by the source, while $\epsilon_j$ is the Dirac $\delta$-function. As before, for the summation to converge, the Green function is smoothed around $r_j$.

The concept of a source blob is conceived in analogy to a vortex blob. The velocity field produced by a source blob is, in effect, the same as that in figure 3. Thus the vel ocity produced in a free space by a source blob at $Z_j$ is given by

$$W_\phi(Z, Z_j) = \frac{\Delta_j\,|Z-Z_j|}{2\pi \max(|Z-Z_j|, r_0)}\,\frac{1}{(Z-Z_j)}. \tag{4.14}$$

The boundary condition expressed by equation (2.9) is satisfied by adding the velocity produced by the image of each source on the other side of the wall. Thus the total velocity produced by a source blob in the $\zeta$-plane is given by

$$W_\epsilon(\zeta, \zeta_j) = W_\phi(\zeta, \zeta_j) + W_\phi(\zeta, \zeta_j^*). \tag{4.15}$$

For $J_s$ source blobs, the solution of equation (4.11) is approximated by the summation specified in equation (4.12), and the corresponding flow velocity is then

$$W_\epsilon(\zeta) = \sum_{j=1}^{J_s} W_\epsilon(\zeta, \zeta_j). \tag{4.16}$$

The strength of the source is adjusted to provide for the volumetric expansion specified by $\Delta_j$ (see equation (4.13)), preserving mass. In one-dimensional flow, as depicted in figure 10,

$$u_s = \tfrac{1}{2}(S_b - S_u), \tag{4.17}$$

where $S_b$ is the flame speed as seen from the burned side and $S_u$ is the flame speed as seen from the unburned side, whence, as a consequence of the continuity requirement,

$$S_b = \nu S_u, \tag{4.18}$$

where

$$\nu \equiv v'_b/v'_u,$$

and one has

$$u_s = \tfrac{1}{2}S_u(\nu - 1). \tag{4.19}$$

The source strength is then

$$\Delta_j = u_s h_c = \tfrac{1}{2}S_u h_c(\nu - 1), \tag{4.20}$$

while the volumetric rate of combustion is given by

$$\mathrm{d}V_\sigma/\mathrm{d}t = h_c S_u = h_c^2 \mathrm{d}f_\sigma/\mathrm{d}t, \tag{4.21}$$

where $\mathrm{d}f_\sigma/\mathrm{d}t$ is the rate of change in $f$ due solely to combustion. This yields

$$\Delta_j = \tfrac{1}{2}h_c^2(\nu - 1)\,\mathrm{d}f_\sigma/\mathrm{d}t. \tag{4.22}$$

At the same time, with reference to figure 3, the source velocity is identified with the velocity of the core,

$$u_0 = \Delta_j/2\pi r_0, \tag{4.23}$$

so that, as a consequence of equation (4.19), one obtains

$$\Delta = 2\pi r_0 u_s = \pi r_0 S_u(\nu - 1). \tag{4.24}$$

Thus, by virtue of equation (4.23), it follows that

$$r_0 = (h_c^2/2\pi S_u k_c)\Delta f_\sigma, \tag{4.25}$$

where the time derivative of $f$ has been expressed in terms of the change in $f$ evaluated for a given time step, $k_c$, by the implementation of the Huygens principle.

By virtue of equation (2.3), volumetric sources affect the velocity field. In particular, they modify the values of $\boldsymbol{u}$. This in turn induces changes in the sheet velocities, as evident from equations (3.24) and (3.27), giving rise to new vortex blobs, etc. The whole algorithm is thus interrelated, as described schematically in figure 3.

### (*d*) *Results*

With the use of the r.v.m. a solution was obtained for turbulent flow with combustion in the tunnel behind a step, modelling the process recorded photographically in figure 1. The exothermicity of the propane–air mixture, with equivalence ratio of 0.5, was for this purpose expressed in terms of the temperature (or specific volume) ratio $\nu = 4.25$, and the laminar burning velocity was taken as $S'_u = 12\ \mathrm{cm\ s^{-1}}$, while, as before, the velocity at inlet was $u'_\infty = 6\ \mathrm{m\ s^{-1}}$ corresponding to $R = 10^4$.

An example of the results is presented in figure 11. Like figure 7, it consists of two sequential series of computer outputs, depicting the variation of vortex velocity vector fields and flame fronts. The flame contour has been delineated for this purpose as a line of demarcation between cells where $f = 0$ and those where $f > 0$. Series ($a$) depicts the process of ignition in the turbulent flow field of figure 7 in a cell located at point (1, 1), i.e., on the centre line of the tunnel at a distance from the step equal to the width of the inlet channel. The sequence in the right column

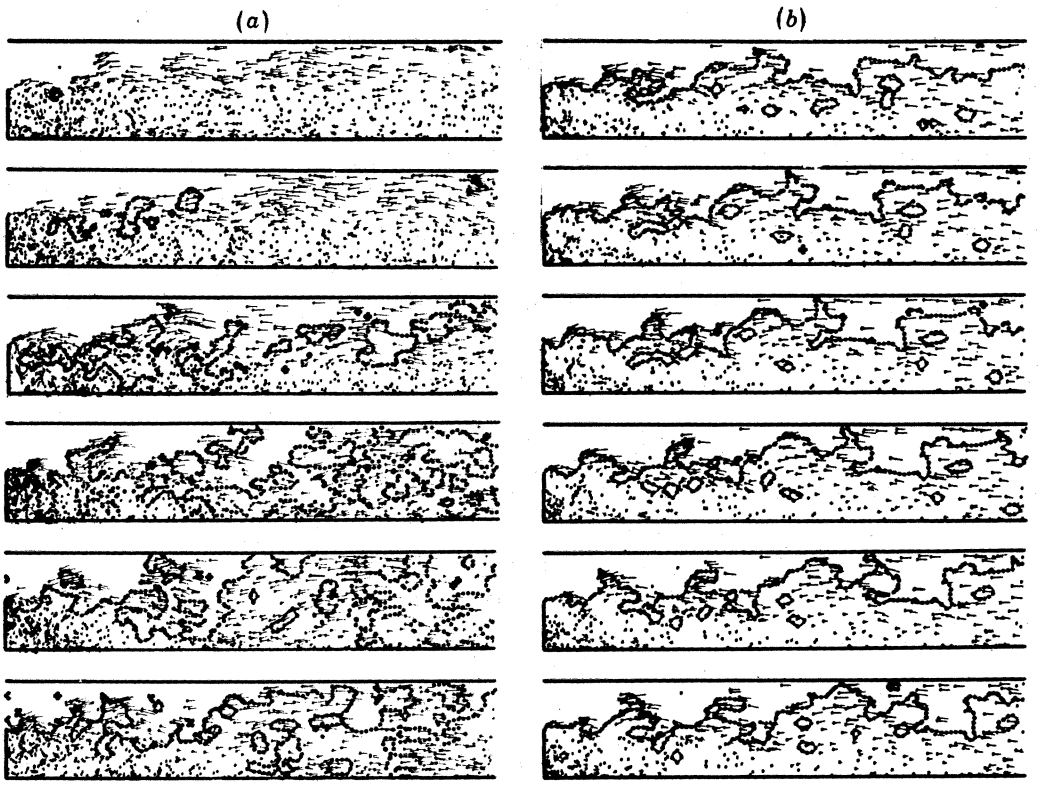


FIGURE 11. Sequential series of computer plots displaying vortex velocity fields and flame fronts in turbulent combustion behind a step at inlet Reynolds numbers $R = 10^4$ while $S_u = 0.02$ and $\nu = 4.25$, corresponding to a propane–air mixture at an equivalence ratio of 0.5; ($a$) ignition at point (1,1) in a fully developed turbulent flow; ($b$) 'steady state' turbulent flame propagation.

displays the 'steady flow condition' attained at time $t' = 26.102(H/2u'_\infty)$ s after ignition at the left bottom corner, point (0, 0), initiated at the moment when the medium was set in motion (hence the smaller number of vortex blobs). The number of computational time steps $0.05(H/2u'_\infty)$ s, between the solutions displayed here was 40 for series ($a$) and four for series ($b$).

In light of the stringent idealizations on which the computations are based, the agreement between the numerical model and the experimental observations is indeed remarkable. The r.v.m. is evidently capable of reproducing the essential features of the flow field associated with turbulent combustion as observed by schlieren photography, providing thereby a clarification of the essential mechanism of the process. At this stage one cannot expect, of course, more than a qualitative agreement. Quantitative modelling of stochastic turbulent flow parameters has to be left for future study.

## 5. Conclusions

The eminent suitability of r.v.m. for the study of the fluid mechanic properties of turbulent combustion has been demonstrated. The main advantage of the method is that it is unencumbered by numerical diffusion. Thus, all the instabilities in the flow field that arise as a characteristic feature of turbulence can be sustained without artificial damping, permitting their effects to be traced without undue distortion. Moreover, by using as the building block the mechanical properties of the essential ingredient of turbulence, the elementary eddy, the r.v.m. is capable of modelling the intrinsic physical properties of the flow system, subject only to restrictions introduced at the outset by the simplifying idealizations.

As a consequence, our analysis displays the following features of turbulent combustion:

(i) fluid mechanical processes of the formation of large-scale turbulent flow structure;

(ii) a rationale for the role played by the intrinsic instability of the flow system in stabilizing the flame, the basic mechanism of a blunt-body flame holder;

(iii) fluid mechanical processes of ignition in turbulent flow of pre-mixed gases;

(iv) detailed features of entrainment and mixing as principal means for the control of the combustion process;

(v) the mechanism of exothermic processes in turbulent combustion.

The authors wish to express their appreciation to the programme director of the research project under which these studies were in part conducted, Dr C. J. Marek of NASA Research Center, for his encouragement and support.

This work was supported by the Engineering, Mathematical, and Geoscience Division of the Department of Energy under contract W-7405-ENG-48, and by the National Aeronautics and Space Administration under NASA grant NSG-3227.

## Appendix 1. Vortex motion in the transformed plane

Trajectories of the vortices in the transformed $\zeta$-plane are required for the evaluation of the velocity $W(Z)$ with the use of equations (3.10) and (3.12). This can be obtained by a stepwise conformal mapping of trajectories in the $Z$-plane, defined by equation (3.17), with the use of the inverse of the transformation function $Z = Z(\zeta)$, the integral form of equation (3.11):

$$Z(\zeta) = \int \frac{\mathrm{d}\zeta}{F(\xi)}, \tag{A 1.1}$$

which, for the geometry of figure 6, is

$$Z = \frac{H}{\pi}\left(\ln\frac{1+q}{1-q} - \tfrac{1}{2}\ln\frac{2+q}{1-q}\right), \tag{A 1.1a}$$

where

$$q = (4-\zeta)/(1-\zeta).$$

However, the inverse of the foregoing,

$$\zeta = \zeta(Z), \tag{A 1.2}$$

is awkward and time-consuming to evaluate. Hence one has to resort to numerical methods to integrate equation (3.11) directly to calculate corresponding displacements in the $\zeta$-plane from those in the $Z$-plane.

This procedure can be reduced substantially if one uses equation (3.18) to trace these vortices in the $\zeta$-plane directly, thus eliminating the use of the $Z$-plane except for the presentation of the results. This equation is obtained from equation (3.12) to write $W(Z)$ in terms of $\zeta$ as

$$W^*(Z) = \{W(\zeta)\, F(\zeta)\}^* = W^*(\zeta)\, F^*(\zeta). \tag{A 1.3}$$

If $\zeta(t)$ is defined to be the map of $Z(t)$, then

$$\zeta(t) = \zeta(Z(t)), \tag{A 1.4}$$

and one can write $$\xi(t+k) - \zeta(t) = \zeta(Z(t+k)) - \zeta(Z(t)),$$

or, taking the first term of the Taylor series expansion,

$$\zeta(t+k) - \zeta(t) = \{Z(t+k) - Z(t)\}\, \mathrm{d}\zeta/\mathrm{d}Z. \tag{A 1.5}$$

If $Z$ is a vortex centre, then equation (3.17) specifies the change in $Z_j$. Using equations (A 1.3) and (3.11) and rearranging, one obtains equation (3.18) as

$$\zeta_j(t+k) = \zeta_j(t) + \{W^*(\zeta_j)\, F^*(\zeta_j)\, k + \eta_j\}\, F(\zeta_j). \tag{A 1.6}$$

Equations (A 1.6) and (3.10) provide all the necessary information about the flow field. Interestingly, the effect of the $Z$-plane geometry on the motion in the $\zeta$-plane is preserved in terms of $F$ and $F^*$ in equation (A 1.6).

## Appendix 2. Derivation of equation (4.23)

The total volume created by a set of sources distributed on the surface of a flame should provide for extra volume on the side of the products owing to the expansion of reactants as they burn. If the fluid leaves a source with a velocity $u_s$ normal to the surface of the flame, then

$$\frac{\mathrm{d}V}{\mathrm{d}t} = \int_f u_s \boldsymbol{n}_f \cdot \mathrm{d}\boldsymbol{A}_f, \tag{A 2.1}$$

where $\mathrm{d}V/\mathrm{d}t$ is the rate of volume increase due to the sources, and $\boldsymbol{A}_f$ is the area of the flame surface. For two-dimensional flow, $\mathrm{d}\boldsymbol{A}_f$ is equal to $\boldsymbol{n}_f \mathrm{d}L_f$, where $L_f$ is the length of the flame front, and both $V$ and $\boldsymbol{A}_f$ are measured per unit length normal to the plane of the flow. Since $u_s$ is constant for homogeneous systems as indicated by equation (4.18), it follows that

$$\frac{\mathrm{d}V}{\mathrm{d}t} = u_s \int_f \boldsymbol{n}_f \cdot \boldsymbol{n}_f \mathrm{d}L_f = u_s L_f. \tag{A 2.2}$$

Flame propagation by combustion, the reason for volume expansion, is expressed by the left-hand side of equation (1.5):

$$\partial \boldsymbol{r}_f / \partial t = \boldsymbol{n}_f S_u. \tag{A 2.3}$$

When integrating the equation (A 2.1) for the flame surface $A_f$, the volumetric rate of combustion is specified as

$$\int_f \frac{\partial \boldsymbol{r}_f}{\partial t} \cdot \mathrm{d}\boldsymbol{A} = \int_f S_u \boldsymbol{n}_f \cdot \mathrm{d}\boldsymbol{A}. \tag{A 2.4}$$

The left side of equation (A 2.4) can be written as

$$\frac{\mathrm{d}V_b}{\mathrm{d}t} = \int_f \frac{\partial \boldsymbol{r}_f}{\partial t}\, \mathrm{d}\boldsymbol{A}_f = \sum_{i,j} h_c^2 \frac{\mathrm{d}f_\sigma}{\mathrm{d}t}, \tag{A 2.5}$$

where $i$ and $j$ cover the whole field of a planar flow. The integral on the right side of equation (A 2.4) is evaluated by assuming a constant $S_u$, yielding an expression similar to the right side of equation (A 2.2). Thus equation (A 2.4) becomes

$$\sum_{i,j} h_c^2 \frac{df_\sigma}{dt} = S_u L_f. \tag{A 2.6}$$

One can write

$$\frac{dV}{dt} = \sum_{i,j} \Delta_{ij}$$

and by eliminating $L_f$ between equations (A 2.6) and (1.2) it follows that

$$\Delta = \frac{u_s}{S_u} h_c^2 \frac{df_\sigma}{dt}. \tag{A 2.7}$$

However, from equations (4.18) and (4.19), one has

$$u_s = \tfrac{1}{2} S_u (\nu - 1),$$

and equation (4.22) follows immediately. By using equation (A 2.7), one avoids calculating the flame length as required by equation (A 2.2). Instead, one uses the computations of the combustion step in the flame propagation algorithm, described before, to obtain the rate of change in the volume due to combustion, as indicated in equation (A 2.5).

## Appendix 3. Conservation of circulation in a variable density field

The flame front, according to the model presented here, is a constant-pressure discontinuity across which a sudden change in density takes place. Of crucial importance to our modelling technique is the fact that vortex blobs conserve their circulation upon crossing this discontinuity. Provided here is a proof of this property, restricted to two-dimensional geometry.

In a two-dimensional potential flow, with variable density, the vortex transport equation (see, for example, equation (4.6) in Chorin & Marsden (1979)),

$$D(\xi/\rho)/Dt = 0, \tag{A 3.1}$$

expresses the variation of vorticity with density along a particle path. However, the variation of the circulation, given by

$$\frac{D\Gamma}{Dt} = \frac{D}{Dt} \int \xi \, dA = \frac{D}{Dt} \int (\xi/\rho) \, \rho \, dA, \tag{A 3.2}$$

can be calculated by reversing the integration and differentiation in the above expression. Thus

$$\frac{D\Gamma}{Dt} = \int \frac{D(\xi/\rho)}{Dt} \rho \, dA + \int (\xi/\rho) \frac{D(\rho \, dA)}{Dt}. \tag{A 3.3}$$

However, $\rho \, dA$ is constant along a particle path and taking equation (A 3.1) into account, we obtain

$$D\Gamma/Dt = 0. \tag{A 3.4}$$

Hence, since vortex blobs follow particle paths, their circulation in a variable-density field is invariant.

## References


Ashurst, W. T. 1979 Numerical simulation of turbulent mixing layers via vortex dynamics. *Proc. 1st Symp. on Turbulent Shear Flows* (ed. by Durst *et al.*), pp. 402–413. Berlin: Springer-Verlag.

Ashurst, W. T. 1981 Vortex simulation of a Model Turbulent Combustor. *Proc. 7th Colloquium on Gas Dynamics of Explosions and Ractive Systems. Prog. Astronaut. Aeronaut.* **76**, 259–273.

Batchelor, G. K. 1967 *An introduction to fluid mechanics*. Cambridge University Press.

Chorin, A. J. 1973 Numerical studies of slightly viscous flow. *J. Fluid Mech.* **57**,785–796.

Chorin, A. J. 1978 Vortex sheet approximation of boundary layers. *J. comput. Phys.* **27**, 428–442.

Chorin, A. J. 1980*a* Vortex models and boundary layer instability. SIAM *Jl scient. Stat. Comput.* **1**, 1–24.

Chorin, A. J. 1980*b* Flame advection and propagation algorithms. *J. comput. Phys.* **35**, 1–11.

Chorin, A. J., Hughes, T. J. R., McCracken, M. F. & Marsden, J. E. 1978 Product formulas and numerical algorithms. *Communs pure appl. Math.* **31**, 205–256.

Chorin, A. J. & Marsden, J. E. 1979 *A mathematical introduction to fluid mechanics*. Berlin: Springer-Verlag.

Cheer, A. Y. 1979 A study of incompressible 2-D vortex flow past a circular cylinder. Lawrence Berkeley Laboratory, LBL-9950.

Ganji, A. R. & Sawyer, R. F. 1980 An experimental study of the flow field of a two-dimensional premixed turbulent flame. *AIAA Jl.* (In the press.)

Hald, O. H. 1979 Convergence of vortex methods for Euler's equations. II. *SIAM Jl numer. Anal.* **16**, 5, 726–755.

Lie, S. & Engel, F. 1880 *Theorie der Transformationsgruppen* (three vols). Leipzig: Teubner.

McCracken, M. & Peskin, C. 1980 Vortex methods for blood flow through heart valves. *J. comput. Phys.* **35**, 183–205.

McDonald, H. 1979 Combustion modeling in two and three dimensions – some numerical considerations. *Prog. Energy Combust. Sci.* **5**, 97–122.

Mellor, A. M. 1979 Turbulent-combustion interaction models for practical high intensity combustors. In *17th Symposium (International) on Combustion*, pp. 377–387. Pittsburgh: The Combustion Institute.

Noh, W. T. & Woodward, P. 1976 SLIC (Simple line interface calculation). *Proc. 5th Int. Conf. Numer. Math. Fluid Mechanics*, pp. 330–339. Berlin: Springer-Verlag.

Roshko, A. 1976 Structure of turbulent shear flows: a new look. *AIAA Jl* **14**, 10, 1349–1357.

Samarski, A. A. 1962 An efficient method for multi-dimensional problems in an arbitrary domain. *Zh. Vych. Mat. mat. Fiz.* **2**, 787–811 (transl. as *U.S.S.R. Comput. Math. & Math. Phys.* 1963, 894–896 (1964)).

Williams, F. A. 1974 A review of some theoretical considerations of turbulent flame structure. Specialists meeting on Analytical and Numerical Methods for Investigation of Flow Fields with Chemical Reaction, Especially Related to Combustion. *AGARD PEP 43rd Meetings*, vol. II, p. 1, Liège, Belgium, pp. 1–125.

Williams, F. A. & Libby, P. A. (ed.) 1980 *Turbulent reacting flows. Topics in applied physics* **4**. Berlin, Heidelberg, New York: Springer-Verlag.




PHILOSOPHICAL TRANSACTIONS OF THE ROYAL SOCIETY A MATHEMATICAL, PHYSICAL & ENGINEERING SCIENCES

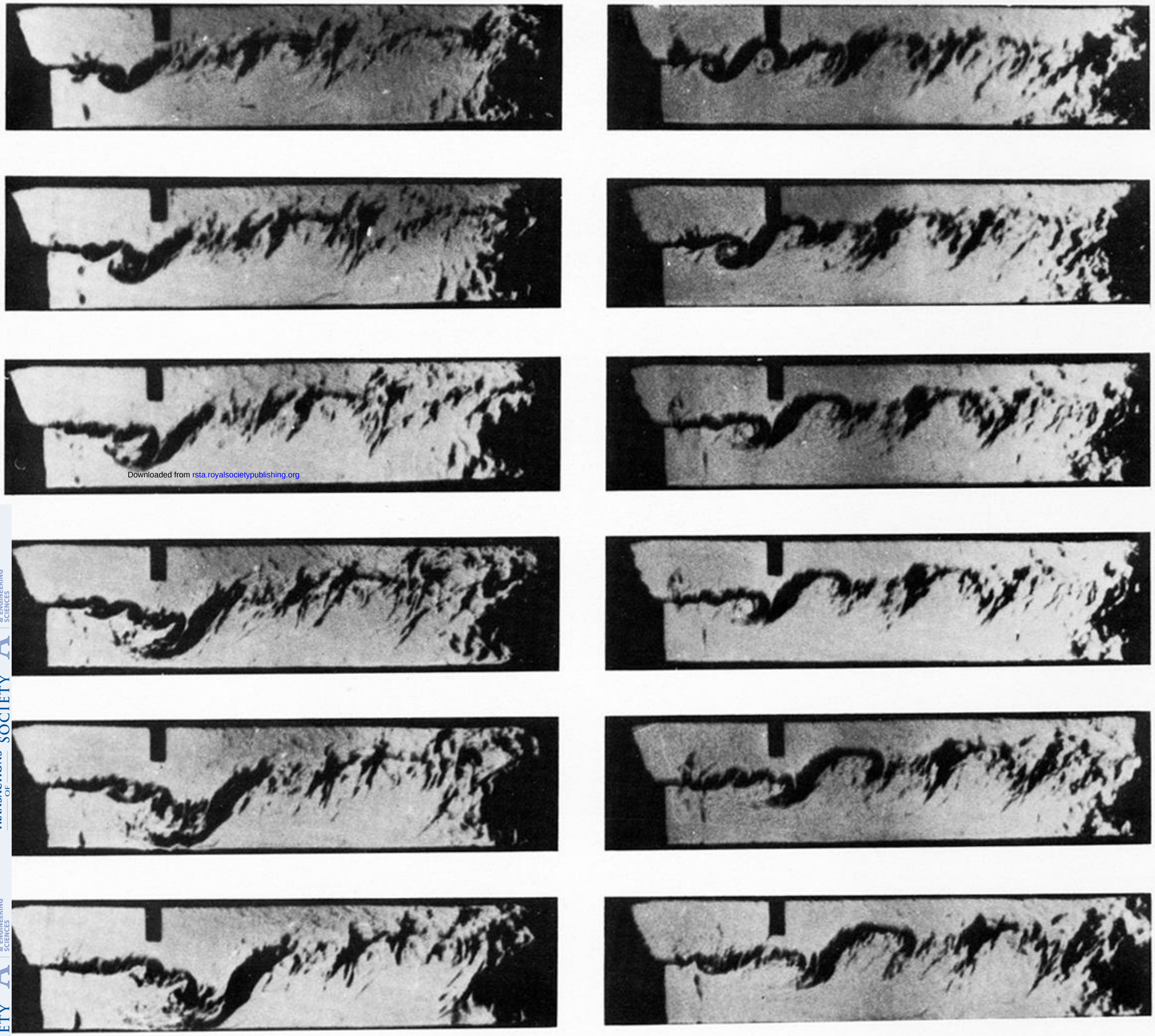


FIGURE 1. Photographic schlieren records of turbulent combustion stabilized behind a step, in a propane–air mixture at an equivalence ratio of 0.57, entering the channel at $u'_\infty = 13.6\ \mathrm{m\ s^{-1}}$ ($R = 22 \times 10^4$) while $T_\infty = 295\ \mathrm{K}$: (*a*) growth of a large eddy under the influence of recirculation (time interval between frames: 1.22 ms); (*b*) 'steady-state' propagation of a large-scale ('coherent') structure (time interval between frames: 1.16 ms).